

Depth Matters: Exploring Deep Interactions of RGB-D for Semantic Segmentation in Traffic Scenes

Siyu Chen^{1*}, Ting Han^{2*}, Changshe Zhang³, Weiquan Liu¹, Jinhe Su^{1†}, Zongyue Wang¹, Guorong Cai^{1†}

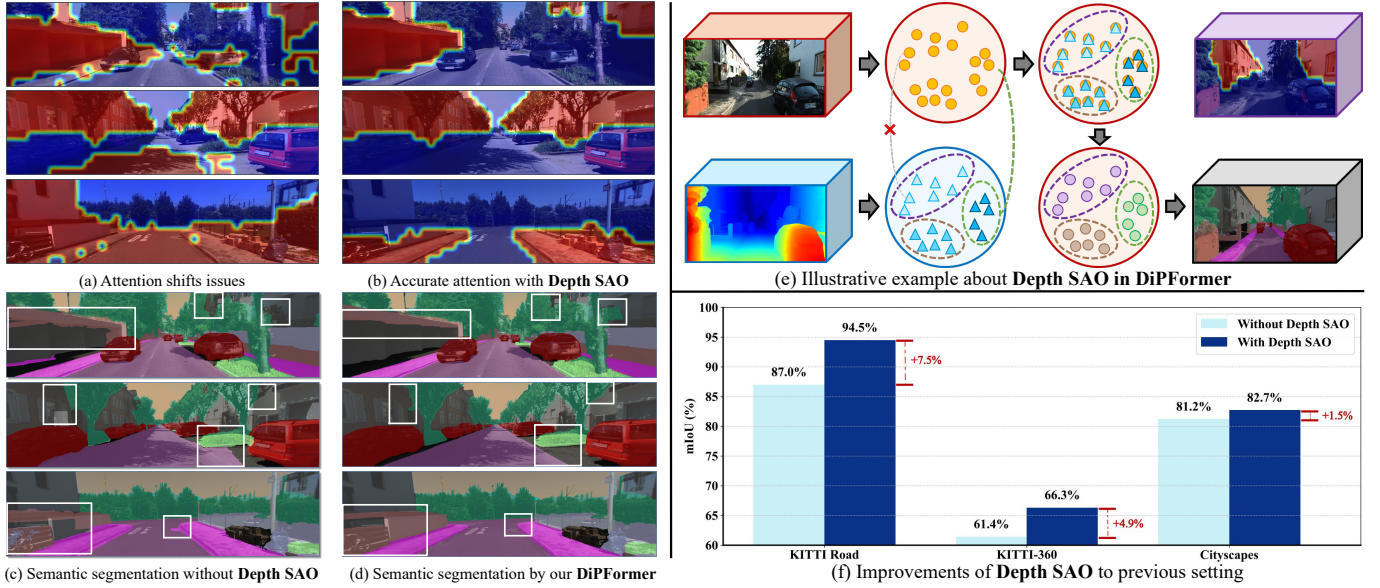


Fig. 1: Effectiveness of **Depth SAO** on attention and semantic segmentation quality.

Abstract—RGB-D has gradually become a crucial data source for understanding complex scenes in assisted driving. However, existing studies have paid insufficient attention to the intrinsic spatial properties of depth maps. This oversight significantly impacts the attention representation, leading to prediction errors caused by attention shift issues. To this end, we propose a novel learnable Depth interaction Pyramid Transformer (DiPFormer) to explore the effectiveness of depth. Firstly, we introduce Depth Spatial-Aware Optimization (Depth SAO) as offset to represent real-world spatial relationships. Secondly, the similarity in the feature space of RGB-D is learned by Depth Linear Cross-Attention (Depth LCA) to clarify spatial differences at the pixel level. Finally, an MLP Decoder is utilized to effectively fuse multi-scale features for meeting real-time requirements. Comprehensive experiments demonstrate that the proposed DiPFormer significantly addresses the issue of attention misalignment in both road detection (+7.5%) and semantic segmentation (+4.9% / +1.5%) tasks. DiPFormer achieves state-of-the-art performance on the KITTI (97.57% F-score on KITTI road and 68.74% mIoU on KITTI-360) and Cityscapes (83.4% mIoU) datasets.

I. INTRODUCTION

With the rapid development of autonomous driving, the ability to accurately understand complex traffic scenes has become increasingly crucial. Traditional single-sensor data often fail short under varying lighting conditions and with dynamic objects. To overcome these challenges, combining texture information with spatial geometry, RGB-D based approaches [1], [2], [3] have emerged as the mainstream methods.

However, existing methods often treat depth information as auxiliary and overlook the intrinsic properties of depth

maps. As a result, conflicts between RGB and depth map in sensitive regions lead to misalignment in the learned attention maps, significantly affecting perception in complex real-world scenes. For instance, the attention shift shown in Fig. 1(a, b) leads to substantial prediction errors.

We believe that depth information plays a more crucial role in multi-modal semantic segmentation. To this end, we propose a novel learnable Depth interaction Pyramid Transformer (DiPFormer) to explore the effectiveness of depth. Firstly, we introduce Depth Spatial-Aware Optimization (**Depth SAO**) to represent spatial relationship characteristics. Secondly, we utilize Depth Linear Cross Attention (**Depth LCA**) to calculate the similarity of RGB-D. The interaction of feature spaces constructs the latent connections between images and the real world, and addresses the attention shift issues, as shown in Fig. 1(e). Multi-scale spatial relationships are generated to adapt to complex scenes across multiple scales. Finally, multi-scale features are further fused in the MLP decoder in a more efficient manner.

Comprehensive experiments demonstrate that the DiPFormer significantly **provides the accurate attention** and improves the segmentation performance, as shown in Fig. 1(c, d). Specifically, Depth SAO significantly enhances segmentation performance, improving by 7.5%, 4.9%, and 1.5% on datasets KITTI Road, KITTI-360, and Cityscapes, respectively (See Fig. 1(f)). Meanwhile, DiPFormer achieves state-of-the-art (SOTA) performance (**97.57% F-score in KITTI Road, 68.74% and 83.4% mIoU in KITTI-360 and Cityscapes,**

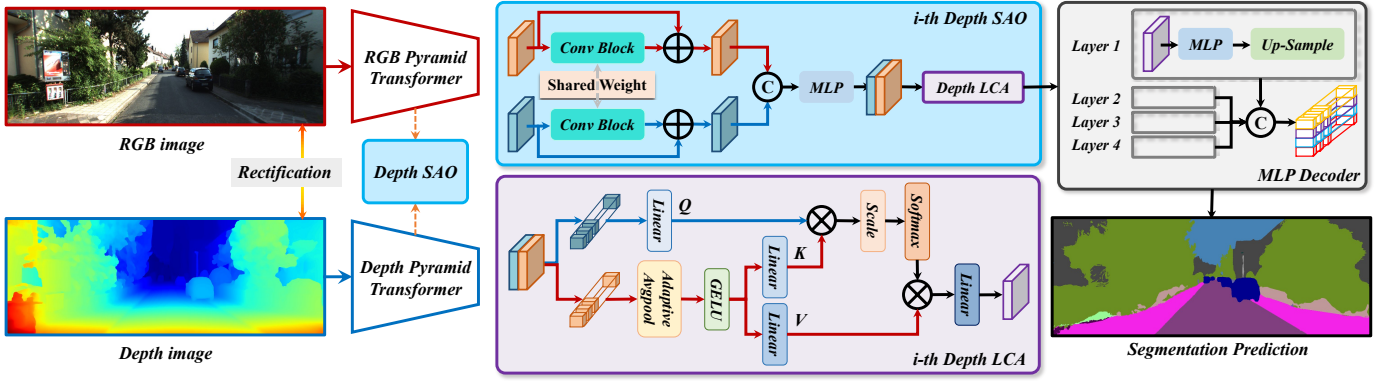


Fig. 2: The overall framework of the proposed DiPFormer, which consists of layer-wise Depth SAO with Depth LCA, and MLP Decoder, for efficient and robust semantic segmentation.

respectively) on the three datasets, further highlighting the importance of depth information. The contributions are as follows:

- We propose a novel learnable Depth interaction Pyramid Transformer that sufficiently integrates spatial information to address attention drift issues.
- The interaction of feature spaces with spatial relationship characteristics constructs the latent connections between images and real world.
- The proposed method achieves Top-1 mIoU and F-score on the three well-known real world datasets with robustness and effectiveness.

II. RELATED WORK

Semantic Segmentation. Previous semantic segmentation methods typically relied on the efficient CNN as backbone for feature extraction [4], [5], [6]. However, due to the limitations of local representations, many methods adopt Vision Transformer for dense prediction [7], [8], [9]. To overcome the challenges that RGB images face under different weather and lighting conditions, multi-modal approaches have gained popularity and are now widely applied in the field of autonomous driving [10], [11], [12]. CMX [13] and CMNeXt [14] have introduced multiple attention modules to facilitate cross-modal learning between visual modalities. Nevertheless, these methods suffer from attention shift issues due to the neglect of the spatial properties of depth information. To this end, we propose Depth SAO and Depth LCA to correct attention shift without additional complex designs.

Road Detection. Road detection is a critical application of semantic segmentation in autonomous driving. Alongside the development of semantic segmentation, road detection also requires spatial information to assist with RGB feature extraction [15], [16], [17]. RGB-L methods project point cloud onto the image plane for feature fusion [18], [19], [20], but they must address challenges related to computational complexity and registration issues. RGB-D methods extract and fuse features in parallel using CNNs or Transformer [21], [22], [23]. These methods aim to provide richer feature

representations but present errors where the two modalities conflict. Our goal is to explore the correlations between RGB-D features in the feature space to model the latent relationships between pixels and the real world.

Position Embedding. In Vision Transformer, position embeddings are essential for understanding the positions of image patches within a sequence. Traditional absolute position embeddings capture location information using fixed sine and cosine values [24], [25], [26], [27], while relative position embeddings [28] represent the distance or difference between patches. Furthermore, many studies [29], [30], [31], [32], [27], [33] have introduced convolutions to provide learnable implicit position embeddings. However, there is often a disconnect between these embeddings and the actual scene. To bridge this gap, we propose Depth SAO to establish an effective connection between position embeddings and the real world scenes.

III. METHOD

This paper introduces a novel learnable Depth interaction Pyramid Transformer (DiPFormer) for semantic segmentation. As shown in Fig. 2, DiPFormer consists of three main modules: Depth SAO, Depth LCA, and MLP decoder. DiPFormer formalizes the relationship between image feature spaces and spatial structure into depth spatial-aware. We details the designs as follows.

A. DiPFormer

Pyramid Transformer DiPFormer takes RGB images and depth maps of identical resolution as input. For an input image of size $H \times W \times 3$, the model first generates multi-level RGB and Depth features, with resolutions of $\frac{1}{2}$, $\frac{1}{4}$, $\frac{1}{8}$, and $\frac{1}{16}$, respectively. The extracted depth features are utilized as position embeddings in Depth SAO to address the attention shift caused by insufficient spatial guidance. This ensures effective alignment between the attention mechanism and the geometric structure of the scene. Subsequently, we employ Depth LCA to perform feature interaction in different feature spaces and obtain the latent spatial difference of pixels. Finally, the MLP decoder progressively restores these multi-level features with

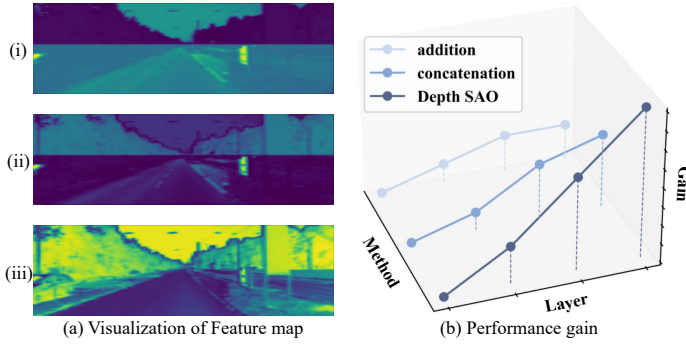


Fig. 3: Visualization the feature maps of different position embedding methods and the performance gain of these methods, where (i), (ii), and (iii) denote the pixel-wise addition, concatenation, and our proposed Depth SAO.

Algorithm 1 Depth Spatial-Aware Optimization Computation

Require: RGB input $\mathbf{R} \in \mathbb{R}^{H \times W \times 3}$,
Depth input $\mathbf{D} \in \mathbb{R}^{H \times W \times 1}$
Ensure: Output feature $\mathbf{F} \in \mathbb{R}^{\frac{H}{2^l} \times \frac{W}{2^l} \times C}$ for each layer
1: **for** each layer $l = 1, \dots, 4$ **do**
2: $\mathbf{R_F}, \mathbf{D_F} \leftarrow \mathbf{R}, \mathbf{D}$
3: **for** $i = 1$ to 3 **do**
4: $\mathbf{R_F}, \mathbf{D_F} \leftarrow \text{GN}(\text{Conv3x3}(\mathbf{R_F}, \mathbf{D_F}))$
5: **if** $i == 1$ **then**
6: $\mathbf{R_F}, \mathbf{D_F} \leftarrow \text{MaxPooling}(\mathbf{R_F}, \mathbf{D_F})$
7: **end if**
8: **end for**
9: $\mathbf{F} \leftarrow \text{Linear}(\mathbf{R_F} + \mathbf{D_F})$
10: **end for**
11: **return** \mathbf{F}

$H \times W \times N_{cls}$, where N_{cls} represents the number of target classes. The predictions are constrained by the cross-entropy loss to acquire accurate semantic segmentation.

B. Depth Spatial-Aware Optimization

Unlike traditional position embeddings, we develop a more sophisticated depth position embedding based on depth features. We carefully consider potential issues such as sparsity and error accumulation that are able to arise during the depth map acquisition process. The position embeddings for pixel-wise addition and concatenation only consider biases, making it difficult to capture global positional relationships, as shown in Fig. 3(a). Since element-wise addition and concatenation amplify errors through iterative attention, we introduce Depth SAO to effectively build spatial offset while ignore noise in the depth information. Error accumulation slows down performance gain, but the proposed DepthSAO overcomes this issue in Fig. 3(b).

Specifically, we design a convolutional block (ConvBlock) with shared parameters to simultaneously learn RGB and depth features. On one hand, the ConvBlock performs Patch Embedding in the Vision Transformer to reduce feature resolution. On the other hand, ConvBlock learns the local RGB-D correspondences and extracts salient features through max-pooling. Subsequently, the RGB-D features are concatenated

and fused through residual connections, and an MLP is used to model the spatial bias relationships. The process of depth SAO is described in Algorithm 1. Depth SAO represents the spatial relationship characteristics between RGB-D in a learnable manner.

C. Depth Linear Cross Attention

We adopt cross-attention mechanism to more effectively manage the interaction between the two modalities. Depth LCA calculates the similarity of RGB-D feature spaces in non-local manner, thereby minimizing the risk of errors. Depth features as learnable position embedding provides valuable prior information about significant spatial relationships for feature extraction. Given the fused feature generated by Depth SAO, both RGB and depth features incorporate biases from the other modality. Therefore, we separate the fused features into new RGB and depth features for subsequent cross-attention.

In Depth LCA, we employ depth features as query and RGB features as key and value since spatial data provides distinctive features between pixels. Therefore, depth queries represent local spatial structural relationships while implicitly capturing the connection between pixels and the real world. Firstly, the depth feature D_F is passed through a linear transformation to obtain the query matrix Q . Concurrently, the RGB feature R_F undergoes an average pooling operation, followed by a linear transformation to generate the key matrix K and the value matrix V . Average pooling is used to extract general features from RGB images. This process is mathematically expressed as:

$$\begin{aligned} Q &= \text{Linear}(D_F); \\ K, V &= \text{Linear}(\text{AvgPool}(R_F)); \end{aligned} \quad (1)$$

The attention effectively combines the global information from the RGB features with the local information from the depth features. In this formula, the dot product $Q \cdot K^T$ between the query matrix Q and the key matrix K is computed for explore the similarity of RGB-D feature spaces. The scale factor *scale* is employed to balance the influence of features from different modalities. The similarity attention is then normalized using the *softmax* to generate the attention weight matrix. The weights are subsequently applied to the value matrix V to achieve the sufficient fusion of RGB-D feature spaces. It is denoted as:

$$\text{Attention}(Q, K, V) = \text{softmax}(Q \cdot K^T \times \text{scale}) \cdot V \quad (2)$$

Following the traditional Transformer architecture, we incorporate num_h head spaces into Depth LCA. The attention from multiple heads is aggregated by \oplus to enhance feature representation.

Depth LCA effectively integrates RGB-D information and captures interactions from different feature spaces. The semantic features obtained through depth queries are represented as latent code with spatial and texture similarity. More importantly, the latent code creates a bridge between pixels and the real world, significantly mitigating attention shift issues. As a result, it alleviates the perception inconsistency in

TABLE I: Evaluation results in Urban Road Benchmark [34]. The best results are in **bold**.

Method	Modal	MaxF (%) \uparrow	AP(%) \uparrow	PRE(%) \uparrow	REC(%) \uparrow	FPR(%) \downarrow	FNR(%) \downarrow	Runtime(s) \downarrow
CLCFNet(2021)[18]	RGB-L	96.38	90.85	96.38	96.39	1.99	3.61	0.02
PLB-RD(2022)[19]	RGB-L	97.42	94.09	97.30	97.54	1.49	2.46	0.46
3MT-RoadSeg(2023)[35]	RGB-L	96.60	93.90	96.46	96.73	1.95	3.27	0.07
LRDNet+(2022)[20]	RGB-L	96.95	92.22	96.88	97.02	1.72	2.98	-
SNE-RoadSeg(2020)[36]	RGB-D	96.75	94.07	96.90	96.61	1.70	3.39	0.18
NIM-RTFNet(2020)[37]	RGB-D	96.02	94.01	96.43	95.62	1.95	4.38	0.05
DFM-RTFNet(2021)[15]	RGB-D	94.78	94.05	96.62	96.93	1.87	3.07	0.08
SNE-RoadSeg+(2021)[38]	RGB-D	97.50	93.98	97.41	97.58	1.43	2.42	0.08
USNet(2022)[16]	RGB-D	96.89	93.25	96.51	97.27	1.94	2.73	0.02
SNE-RoadSegV2(2023)[21]	RGB-D	97.55	93.98	97.57	97.53	1.34	2.47	0.03
EpurateNet(2024)[22]	RGB-D	97.09	93.08	96.76	97.43	1.89	2.76	0.02
RoadFormer(2024)[23]	RGB-D	97.50	93.85	97.16	97.84	1.57	2.16	0.07
RoadFormer+(2024)[39]	RGB-D	97.56	93.74	97.43	97.69	1.42	2.31	0.04
DiPFormer (Ours)	RGB-D	97.57	92.94	97.34	97.79	1.47	2.21	0.02

regions where modal information conflicts in traditional RGB-D fusion.

D. MLP Decoder

MLP Decoder is a lightweight decoder composed solely of MLP layers, avoiding excessive computational overheads. Meanwhile, the MLP decoder has a larger and more efficient receptive field compared to convolutions. Depth SAO generates multi-scale highly local and non-local interaction features. Firstly, multi-layer features from the Depth SAO are compressed to a uniform number C of channels. Then, they are upsampled at the size of $\frac{H}{4} \times \frac{W}{4} \times C$ individually. Thirdly, aggregation is performed by concatenation. Finally, an additional MLP layer is applied to predict the segmentation mask at the size of $\frac{H}{4} \times \frac{W}{4} \times N_{cls}$ from the fused features. MLP decoder unifies the multi-scale features to produce complementary and powerful representations.

E. Complexity

In Depth LCA, adaptive average pooling reduces the feature dimension from $H \times W \times C$ to $P \times P \times C$. Consequently, the computational complexity of Depth LCA decreases from $O(HWC)$ to $O(P^2C)$, where P is much smaller than H and W . Moreover, the computational complexity of MLP Decoder is $O(HWC_{in}M)$, which is lower compared to the traditional convolutional decoder's complexity of $O(HWC^2)$, where C_{in} and M are much smaller than C . The reduced computational complexity ensures that our design is lightweight and efficient, effectively meeting the real-time demands of traffic scene understanding.

IV. EXPERIMENTS

A. Datasets and Metric

KITTI Road [34]: The KITTI Road Dataset includes 289 training RGB-D image pairs and 290 testing pairs, each with a resolution of $1,242 \times 375$ pixels. It covers three road scenarios: urban unmarked, urban marked, and urban multiple marked

lanes. The Urban Road Benchmark provides the comprehensive road detection evaluation of the three aforementioned road scenes.

KITTI-360 [40]: KITTI-360 is a large-scale street scene dataset, and extends the original KITTI dataset [41]. It includes 49,004 training pairs and 12,276 testing pairs with a resolution of $1,408 \times 376$. The dataset provides dense semantic segmentation annotations across 19 classes.

Cityscapes [42]: Cityscapes is an RGB-D dataset that is used for both road detection and semantic segmentation. It consists of 5,000 image pairs, divided into training, validation, and testing subsets (2,975 / 500 / 1,525). Each image is annotated across 19 categories with a resolution of $2,048 \times 1,024$.

Metric: The performance of road detection is primarily evaluated on the KITTI Road dataset using the Max F1-measure. In addition, metrics such as Precision (PRE), Recall (REC), Intersection Over Union (IoU), Average Precision (AP), False Positive Rate (FPR), False Negative Rate (FNR), and runtimes are also assessed. For the semantic segmentation tasks, the mean Intersection over Union (mIoU) was employed as the evaluation metric on the KITTI-360 and Cityscapes datasets.

B. Implementation Details

Our model training is conducted on four NVIDIA 4090 GPUs, with a batch size of 4 per GPU. Initially, the network model is pre-trained on ImageNet-1K [43]. During training, we apply various data augmentation techniques to enhance the model's generalization capability, including random flipping, random scaling within the range of $[0.5, 2]$, random color jittering, and random Gaussian blur. We opt for the AdamW optimizer with a weight decay of 0.05. The initial learning rate was set to $6e-5$, and a cosine annealing strategy with a warm-up phase was employed for learning rate scheduling.

C. Comprehensive Evaluation

We conduct a comprehensive evaluation of the proposed DiPFormer using the benchmark datasets KITTI Road, KITTI-360, and Cityscapes, respectively. These datasets provide a

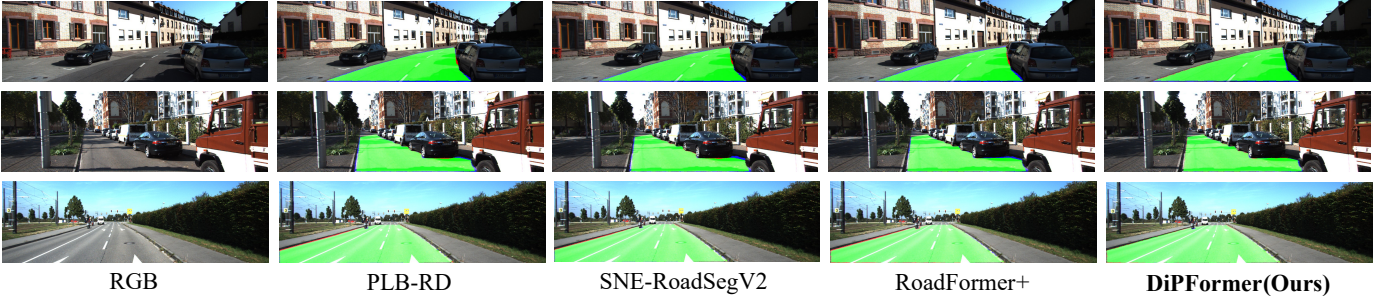


Fig. 4: Qualitative results on KITTI Road [40] compared with latest high-performance methods.

TABLE II: Main results on Cityscapes [40], where mIoU is all categories evaluation and MaxF is road detection evaluation. The best results are in bold.

Method	Modal	mIoU(%) \uparrow	MaxF (%) \uparrow
PVT(2021)[44]	RGB	78.6	-
SegFormer(2021)[45]	RGB	81.0	-
PVTv2(2022)[46]	RGB	80.6	-
HRViT(2022)[47]	RGB	82.8	-
FAN-L-Hybrid(2023)[48]	RGB	82.8	-
SA-Gate(2020)[49]	RGB-D	81.7	-
USNet(2022)[16]	RGB-D	-	98.27
CMX(2023)[13]	RGB-D	82.6	-
DFormer(2023)[50]	RGB-D	74.4	-
SNE-RoadSegV2(2024)[21]	RGB-D	-	97.12
RoadFormer(2024)[23]	RGB-D	76.1	96.56
RoadFormer+(2024)[39]	RGB-D	77.4	97.96
DiPFormer(Ours)	RGB-D	83.4	98.86

TABLE III: Main results on KITTI-360 [40]. The best results are in bold.

Method	Modal	Param(M)	mIoU(%) \uparrow
PVT(2021)[44]	RGB	28.2	57.53
SegFormer(2021)[45]	RGB	25.9	61.37
PVT v2(2022)[46]	RGB	29.1	59.70
TokenFusion(2022)[51]	RGB-L	26.0	54.55
CMX(2023)[13]	RGB-L	66.7	64.31
CMNeXt(2023)[14]	RGB-L	58.7	65.26
PGDENet(2022)[52]	RGB-D	107.0	56.34
TokenFusion(2022)[51]	RGB-D	26.0	57.44
CMX(2023)[13]	RGB-D	66.7	64.43
CMNeXt(2023)[14]	RGB-D	58.7	65.09
DiPFormer(Ours)	RGB-D	56.3	68.74

diverse and challenging environment for assessing the performance in road detection and multi-class semantic segmentation tasks. Moreover, we compare DiPFormer against the current SOTA methods to thoroughly evaluate its advantages and areas of improvement. Note that RGB-L and RGB-D denote the input as RGB images with LiDAR point cloud and depth maps, respectively.

1) **Road Detection:** The Quantitative results on the KITTI Road dataset (see Tab. I) demonstrate that DiPFormer excels across multiple key metrics. Specifically, DiPFormer

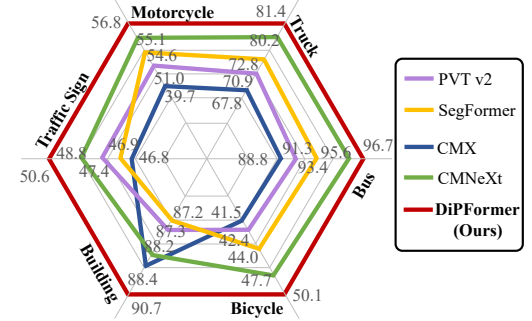


Fig. 5: Comparison of challenging categories in the KITTI-360 dataset [40].

achieves the highest performance in terms of MaxF (97.57%), REC (97.79%), and FNR (2.21%). Compared to previous method, DiPFormer maintains top performance while also being highly competitive in terms of speed. Especially compared to Transformer-based methods, the speed is significantly improved by the efficient attention Depth LCA and MLP Decoder. Qualitative results are shown in Fig. 4, where the scenes are UM, UMM, and UU from top to bottom. DiPFormer achieves the best edge segmentation in road and vehicles contours. Moreover, we conduct the road detection experiment on the Cityscapes dataset. As shown in Tab. II, the proposed method achieves a best MaxF of 98.56%, approximately 0.6% higher than the second-best method.

2) **Semantic Segmentation:** We use Cityscapes and KITTI-360 dataset for the semantic segmentation evaluation. On the Cityscapes dataset (Tab. II), DiPFormer delivers outstanding performance with 83.4% mIoU, surpassing other advanced methods. The depth images from Cityscapes contain inherent noise, which inevitably affect the performance of RGB-D methods. However, the proposed method significantly mitigates error accumulation in depth images by leveraging the similarity in the RGB-D feature space and utilizing learnable depth position embeddings.

In Tab. III, we assess the performance of DiPFormer on the KITTI-360 dataset. DiPFormer achieves a notable mIoU of 68.74% with a modest parameter of 56.3M, significantly outperforming other methods such as CMNeXt (65.26%) and CMX (64.43%). Fig. 5, DiPFormer excels in several chal-

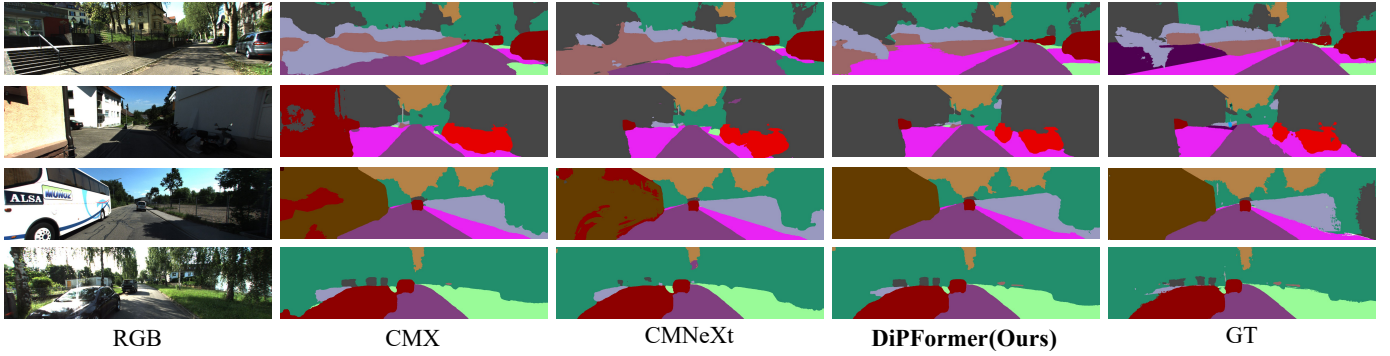


Fig. 6: Qualitative results on KITTI-360 [34] compared with latest high-performance methods.

TABLE IV: Ablation Study of DiPFormer Components.

(a) Depth SAO & LCA analysis.

Components	Param (M)	mIoU (%) \uparrow	mAcc (%) \uparrow
baseline	29.1	59.7	65.0
+Depth SAO	47.8	63.1	70.2
+Depth LCA	40.7	62.3	71.6
+Depth SAO & LCA	59.4	67.1	77.4

(b) MLP Decoder analysis.

Components	Param (M)	mIoU (%) \uparrow	mAcc (%) \uparrow
baseline	29.1	59.7	65.0
w/ MLP Decoder	25.3	61.4	69.0
DiPFormer w/o MLP Decoder	59.4	67.1	77.4
DiPFormer w/ MLP Decoder	56.3	68.7	79.8

TABLE V: Semantic segmentation performance of different position embeddings on KITTI-360 val set. The best results are in bold. We apply different PEs to the PVT v2-B2 [46] to ensure fairness in the comparison.

Position Embeddings	Input	mIoU(%) \uparrow
Sine / Cosine PE[53], [24]	RGB	57.4
Learnable PE[44], [54]	RGB-D	59.1
Implicit PE[46], [45]	RGB-D	62.3
Depth SAO (Ours)	RGB-D	66.3

lenging categories, which are typically difficult to accurately identify in complex traffic scenarios. Fig. 6 demonstrates DiPFormer accurately segments the various objects in complex traffic environments.

D. Ablation Studies

Components analysis of DiPFormer. To evaluate the individual contributes of our designs, we incrementally added each component and assessed their impact. As shown in Tab. IV, the Depth SAO and Depth LCA contribute significantly to the performance improvement. Especially when built upon the SAO, LCA further enhances the interaction within the RGB-D feature space and provide mIoU increasing from 63.1% to 67.1%. The MLP Decoder reduces the parameter by approxi-

mately 3% and improves mIoU by 2% compared with Vanilla. These results demonstrate the efficiency of the MLP Decoder and its ability to provide richer feature representations.

The effectiveness of Depth SAO. Tab. V compares performance across different position embeddings (PE) on the KITTI-360 validation set. The traditional Sine / Cosine PEs achieve an mIoU of 57.4%, the learnable PE reaches 59.1%, and the implicit PE improves to 62.3%. The proposed Depth SAO significantly increases the mIoU to 66.3%, outperforming all other methods and demonstrating the superiority in capturing spatial relationship.

V. CONCLUSIONS

This paper presents the DiPFormer framework, a novel approach for semantic segmentation and road detection in complex real-world traffic environment. First, we develop Depth SAO as learnable position embedding to represent the spatial relationship. Next, we design the Depth LCA to generate the similarity of RGB-D feature spaces and clarify the spatial difference at the pixel level. Lastly, the multi-scale features are efficient fused to provide the dense predictions. Extensive experiments have verified the effectiveness of our designs. Notably, our method constructs the implicit spatial representation to model the correlation between pixels and real world scenes. Our method surpasses previous approaches both on semantic segmentation and road detection tasks in three well-known datasets, demonstrating the advancement of our approach.

Limitations. One notable limitation of our work is still relies on the quality of the depth iamges to some extent. Despite our design mitigates error accumulation, the improvement contributed by sparse depth is not significant, as shown in Fig. 1(f: Cityscapes). Therefore, we will explore an unified framework that integrates segmentation with depth estimation to reduce reliance on depth images and strengthen the relationship between pixels and depth.

ACKNOWLEDGMENT

The authors would like to thank the editor and the anonymous reviewers for their critical and constructive comments and suggestions.

REFERENCES

- [1] J. Piekenbrinck, A. Hermans, N. Vaskevicius, T. Linder, and B. Leibe, "Rgb-d cube r-cnn: 3d object detection with selective modality dropout," in *IEEE Conf. Comput. Vis. Pattern Recog.*, 2024, pp. 1997–2006.
- [2] H. Xia, Y. Fu, S. Liu, and X. Wang, "Rgb-d objects in the wild: Scaling real-world 3d object learning from rgb-d videos," in *IEEE Conf. Comput. Vis. Pattern Recog.*, 2024, pp. 22 378–22 389.
- [3] A. Rajpal, N. Cheema, K. Illgner-Fehns, P. Slusallek, and S. Jaiswal, "High-resolution synthetic rgb-d datasets for monocular depth estimation," in *IEEE Conf. Comput. Vis. Pattern Recog. Worksh.*, June 2023, pp. 1188–1198.
- [4] W. Wang, J. Dai, Z. Chen, Z. Huang, Z. Li, X. Zhu, X. Hu, T. Lu, L. Lu, H. Li, *et al.*, "Internimage: Exploring large-scale vision foundation models with deformable convolutions," in *Proceedings of the IEEE/CVF conference on computer vision and pattern recognition*, 2023, pp. 14 408–14 419.
- [5] Y. Ji, Z. Chen, E. Xie, L. Hong, X. Liu, Z. Liu, T. Lu, Z. Li, and P. Luo, "Ddp: Diffusion model for dense visual prediction," in *Proceedings of the IEEE/CVF International Conference on Computer Vision*, 2023, pp. 21 741–21 752.
- [6] D. Wu, Z. Guo, A. Li, C. Yu, C. Gao, and N. Sang, "Conditional boundary loss for semantic segmentation," *IEEE Transactions on Image Processing*, 2023.
- [7] S. Erisen, "Sernet-former: Semantic segmentation by efficient residual network with attention-boosting gates and attention-fusion networks," *arXiv preprint arXiv:2401.15741*, 2024.
- [8] L. Yang, B. Kang, Z. Huang, X. Xu, J. Feng, and H. Zhao, "Depth anything: Unleashing the power of large-scale unlabeled data," in *Proceedings of the IEEE/CVF Conference on Computer Vision and Pattern Recognition*, 2024, pp. 10 371–10 381.
- [9] J. Jain, J. Li, M. T. Chiu, A. Hassani, N. Orlov, and H. Shi, "Oneformer: One transformer to rule universal image segmentation," in *Proceedings of the IEEE/CVF Conference on Computer Vision and Pattern Recognition*, 2023, pp. 2989–2998.
- [10] D. Feng, C. Haase-Schütz, L. Rosenbaum, H. Hertlein, C. Glaeser, F. Timm, W. Wiesbeck, and K. Dietmayer, "Deep multi-modal object detection and semantic segmentation for autonomous driving: Datasets, methods, and challenges," *IEEE Transactions on Intelligent Transportation Systems*, vol. 22, no. 3, pp. 1341–1360, 2020.
- [11] T. Ye, W. Jing, C. Hu, S. Huang, L. Gao, F. Li, J. Wang, K. Guo, W. Xiao, W. Mao, *et al.*, "Fusionad: Multi-modality fusion for prediction and planning tasks of autonomous driving," *arXiv preprint arXiv:2308.01006*, 2023.
- [12] D. Fu, W. Lei, L. Wen, P. Cai, S. Mao, M. Dou, B. Shi, and Y. Qiao, "Limsim++: A closed-loop platform for deploying multimodal llms in autonomous driving," *arXiv preprint arXiv:2402.01246*, 2024.
- [13] J. Zhang, H. Liu, K. Yang, X. Hu, R. Liu, and R. Stiefelhagen, "Cmx: Cross-modal fusion for rgb-x semantic segmentation with transformers," *IEEE Transactions on Intelligent Transportation Systems*, 2023.
- [14] J. Zhang, R. Liu, H. Shi, K. Yang, S. Reiß, K. Peng, H. Fu, K. Wang, and R. Stiefelhagen, "Delivering arbitrary-modal semantic segmentation," in *IEEE Conf. Comput. Vis. Pattern Recog.*, 2023, pp. 1136–1147.
- [15] H. Wang, R. Fan, Y. Sun, and M. Liu, "Dynamic fusion module evolves drivable area and road anomaly detection: A benchmark and algorithms," *IEEE transactions on cybernetics*, vol. 52, no. 10, pp. 10 750–10 760, 2021.
- [16] Y. Chang, F. Xue, F. Sheng, W. Liang, and A. Ming, "Fast road segmentation via uncertainty-aware symmetric network," in *2022 International Conference on Robotics and Automation (ICRA)*. IEEE, 2022, pp. 11 124–11 130.
- [17] J.-Y. Sun, S.-W. Kim, S.-W. Lee, Y.-W. Kim, and S.-J. Ko, "Reverse and boundary attention network for road segmentation," in *Proceedings of the IEEE/CVF International Conference on Computer Vision Workshops*, 2019, pp. 0–0.
- [18] S. Gu, J. Yang, and H. Kong, "A cascaded lidar-camera fusion network for road detection," in *2021 IEEE international conference on robotics and automation (ICRA)*. IEEE, 2021, pp. 13 308–13 314.
- [19] L. Sun, H. Zhang, and W. Yin, "Pseudo-lidar-based road detection," *IEEE Transactions on Circuits and Systems for Video Technology*, vol. 32, no. 8, pp. 5386–5398, 2022.
- [20] A. A. Khan, J. Shao, Y. Rao, L. She, and H. T. Shen, "Lrdnet: lightweight lidar aided cascaded feature pools for free road space detection," *IEEE Trans. Multimedia*, 2022.
- [21] Y. Feng, Y. Ma, Q. Chen, I. Pitas, and R. Fan, "Sne-roadsegv2: Advancing heterogeneous feature fusion and fallibility awareness for freespace detection," *arXiv preprint arXiv:2402.18918*, 2024.
- [22] T. Han, S. Chen, C. Li, Z. Wang, J. Su, M. Huang, and G. Cai, "Epurate-net: Efficient progressive uncertainty refinement analysis for traffic environment urban road detection," *IEEE Transactions on Intelligent Transportation Systems*, 2024.
- [23] J. Li, Y. Zhan, P. Yun, G. Zhou, Q. Chen, and R. Fan, "Roadformer: Duplex transformer for rgb-normal semantic road scene parsing," *IEEE Transactions on Intelligent Vehicles*, 2024.
- [24] A. Vaswani, N. Shazeer, N. Parmar, J. Uszkoreit, L. Jones, A. N. Gomez, Ł. Kaiser, and I. Polosukhin, "Attention is all you need," *Advances in neural information processing systems*, vol. 30, 2017.
- [25] N. Carion, F. Massa, G. Synnaeve, N. Usunier, A. Kirillov, and S. Zagoruyko, "End-to-end object detection with transformers," in *European conference on computer vision*. Springer, 2020, pp. 213–229.
- [26] H. Zhang, F. Li, S. Liu, L. Zhang, H. Su, J. Zhu, L. M. Ni, and H.-Y. Shum, "Dino: Detr with improved denoising anchor boxes for end-to-end object detection," *arXiv preprint arXiv:2203.03605*, 2022.
- [27] Q. Zhang, Y. Xu, J. Zhang, and D. Tao, "Vitaev2: Vision transformer advanced by exploring inductive bias for image recognition and beyond," *International Journal of Computer Vision*, vol. 131, no. 5, pp. 1141–1162, 2023.
- [28] Z. Liu, H. Hu, Y. Lin, Z. Yao, Z. Xie, Y. Wei, J. Ning, Y. Cao, Z. Zhang, L. Dong, *et al.*, "Swin transformer v2: Scaling up capacity and resolution," in *Proceedings of the IEEE/CVF conference on computer vision and pattern recognition*, 2022, pp. 12 009–12 019.
- [29] Q. Fan, H. Huang, M. Chen, H. Liu, and R. He, "Rmt: Retentive networks meet vision transformers," in *Proceedings of the IEEE/CVF Conference on Computer Vision and Pattern Recognition*, 2024, pp. 5641–5651.
- [30] J. Jiao, Y.-M. Tang, K.-Y. Lin, Y. Gao, A. J. Ma, Y. Wang, and W.-S. Zheng, "Dilateformer: Multi-scale dilated transformer for visual recognition," *IEEE Transactions on Multimedia*, vol. 25, pp. 8906–8919, 2023.
- [31] Q. Fan, H. Huang, X. Zhou, and R. He, "Lightweight vision transformer with bidirectional interaction," *Advances in Neural Information Processing Systems*, vol. 36, 2024.
- [32] X. Lu, M. Suganuma, and T. Okatani, "Sbcformer: Lightweight network capable of full-size imagenet classification at 1 fps on single board computers," in *Proceedings of the IEEE/CVF Winter Conference on Applications of Computer Vision*, 2024, pp. 1123–1133.
- [33] J. Zhang, X. Li, Y. Wang, C. Wang, Y. Yang, Y. Liu, and D. Tao, "Eatformer: Improving vision transformer inspired by evolutionary algorithm," *International Journal of Computer Vision*, pp. 1–28, 2024.
- [34] B. Wang, V. Frémont, and S. A. Rodríguez, "Color-based road detection and its evaluation on the kitti road benchmark," in *2014 IEEE Intelligent Vehicles Symposium Proceedings*. IEEE, 2014, pp. 31–36.
- [35] E. Milli, Ö. Erkan, and A. E. Yılmaz, "Multi-modal multi-task (3mt) road segmentation," *IEEE Robotics and Automation Letters*, 2023.
- [36] R. Fan, H. Wang, P. Cai, and M. Liu, "Sne-roadseg: Incorporating surface normal information into semantic segmentation for accurate freespace detection," in *Computer Vision–ECCV 2020: 16th European Conference, Glasgow, UK, August 23–28, 2020, Proceedings, Part XXX 16*. Springer, 2020, pp. 340–356.
- [37] H. Wang, R. Fan, Y. Sun, and M. Liu, "Applying surface normal information in drivable area and road anomaly detection for ground mobile robots," in *2020 IEEE/RSJ International Conference on Intelligent Robots and Systems (IROS)*. IEEE, 2020, pp. 2706–2711.
- [38] H. Wang, R. Fan, P. Cai, and M. Liu, "Sne-roadseg+: Rethinking depth-normal translation and deep supervision for freespace detection," in *2021 IEEE/RSJ International Conference on Intelligent Robots and Systems (IROS)*. IEEE, 2021, pp. 1140–1145.
- [39] J. Huang, J. Li, N. Jia, Y. Sun, C. Liu, Q. Chen, and R. Fan, "Roadformer+: Delivering rgb-x scene parsing through scale-aware information decoupling and advanced heterogeneous feature fusion," *IEEE Transactions on Intelligent Vehicles*, 2024.
- [40] Y. Liao, J. Xie, and A. Geiger, "KITTI-360: A novel dataset and benchmarks for urban scene understanding in 2d and 3d," *IEEE Trans. Pattern Anal. Mach. Intell.*, 2022.
- [41] A. Geiger, P. Lenz, C. Stiller, and R. Urtasun, "Vision meets robotics: The kitti dataset," *The International Journal of Robotics Research*, 2013.

- [42] M. Cordts, M. Omran, S. Ramos, T. Rehfeld, M. Enzweiler, R. Benenson, U. Franke, S. Roth, and B. Schiele, "The cityscapes dataset for semantic urban scene understanding," in *IEEE Conf. Comput. Vis. Pattern Recog.*, 2016.
- [43] J. Deng, W. Dong, R. Socher, L.-J. Li, K. Li, and L. Fei-Fei, "Imagenet: A large-scale hierarchical image database," in *IEEE Conf. Comput. Vis. Pattern Recog.*, Ieee, 2009, pp. 248–255.
- [44] W. Wang, E. Xie, X. Li, D.-P. Fan, K. Song, D. Liang, T. Lu, P. Luo, and L. Shao, "Pyramid vision transformer: A versatile backbone for dense prediction without convolutions," in *Proceedings of the IEEE/CVF international conference on computer vision*, 2021, pp. 568–578.
- [45] E. Xie, W. Wang, Z. Yu, A. Anandkumar, J. M. Alvarez, and P. Luo, "Segformer: Simple and efficient design for semantic segmentation with transformers," *Advances in Neural Information Processing Systems*, vol. 34, pp. 12 077–12 090, 2021.
- [46] W. Wang, E. Xie, X. Li, D.-P. Fan, K. Song, D. Liang, T. Lu, P. Luo, and L. Shao, "Pvt v2: Improved baselines with pyramid vision transformer," *Computational Visual Media*, vol. 8, no. 3, pp. 415–424, 2022.
- [47] J. Gu, H. Kwon, D. Wang, W. Ye, M. Li, Y.-H. Chen, L. Lai, V. Chandra, and D. Z. Pan, "Multi-scale high-resolution vision transformer for semantic segmentation," in *IEEE Conf. Comput. Vis. Pattern Recog.*, 2022, pp. 12 094–12 103.
- [48] B. Zhao, Z. Yu, S. Lan, Y. Cheng, A. Anandkumar, Y. Lao, and J. M. Alvarez, "Fully attentional networks with self-emerging token labeling," in *IEEE Conf. Comput. Vis. Pattern Recog.*, 2023, pp. 5585–5595.
- [49] X. Chen, K.-Y. Lin, J. Wang, W. Wu, C. Qian, H. Li, and G. Zeng, "Bi-directional cross-modality feature propagation with separation-and-aggregation gate for rgb-d semantic segmentation," in *Eur. Conf. Comput. Vis.*, Springer, 2020, pp. 561–577.
- [50] B. Yin, X. Zhang, Z. Li, L. Liu, M.-M. Cheng, and Q. Hou, "Dformer: Rethinking rgb-d representation learning for semantic segmentation," *arXiv preprint arXiv:2309.09668*, 2023.
- [51] Y. Wang, X. Chen, L. Cao, W. Huang, F. Sun, and Y. Wang, "Multimodal token fusion for vision transformers," in *IEEE Conf. Comput. Vis. Pattern Recog.*, 2022, pp. 12 186–12 195.
- [52] W. Zhou, E. Yang, J. Lei, J. Wan, and L. Yu, "Pgdenet: Progressive guided fusion and depth enhancement network for rgb-d indoor scene parsing," *IEEE Trans. Multimedia*, 2022.
- [53] A. Dosovitskiy, L. Beyer, A. Kolesnikov, D. Weissenborn, X. Zhai, T. Unterthiner, M. Dehghani, M. Minderer, G. Heigold, S. Gelly, *et al.*, "An image is worth 16x16 words: Transformers for image recognition at scale," *arXiv preprint arXiv:2010.11929*, 2020.
- [54] L. Yuan, Y. Chen, T. Wang, W. Yu, Y. Shi, Z.-H. Jiang, F. E. Tay, J. Feng, and S. Yan, "Tokens-to-token vit: Training vision transformers from scratch on imagenet," in *Int. Conf. Comput. Vis.*, 2021, pp. 558–567.